Applied Surface Science 320 (2014) 596–601

Contents lists available at ScienceDirect

Applied Surface Science

journal homepage: www.elsevier.com/locate/apsusc

Cytotoxicity of protein corona-graphene oxide nanoribbons on human epithelial cells

Doris A. Mbeh[a], Omid Akhavan[b,c,*], Taraneh Javanbakht[a], Morteza Mahmoudi[d], L'Hocine Yahia[a]

[a] Laboratory for Innovation and Analysis of Bio-Performance, École Polytechnique, C.P. 6079, Succursale Centre-ville, Montréal, Québec H3C 3A7, Canada
[b] Department of Physics, Sharif University of Technology, P.O. Box 11155-9161, Tehran, Iran
[c] Institute for Nanoscience and Nanotechnology, Sharif University of Technology, P.O. Box 14588-89694, Tehran, Iran
[d] Department of Nanotechnology, Faculty of Pharmacy, Tehran University of Medical Sciences, Iran

ARTICLE INFO

Article history:
Received 30 August 2014
Received in revised form
23 September 2014
Accepted 23 September 2014
Available online 30 September 2014

Keywords:
Graphene oxide
Nanoribbons
Protein corona
Cytotoxicity
Human cells

ABSTRACT

Graphene oxide nanoribbons (GONRs) were synthesized using an oxidative unzipping of multi-walled carbon nanotubes. The interactions of the GONRs with various concentrations of fetal bovine serum or human plasma serum indicated that the GONRs were functionalized substantially by the albumin originated from the two different protein sources. Then, concentration-dependent cytotoxicity of the protein-functionalized GONRs on human epithelial cells was studied. Although the GONRs with concentrations ≤50 μg/mL did not exhibit significant cytotoxicity on the cells (with the cell viability >85%), the concentration of 100 μg/mL exhibited significant cytotoxicity including prevention of cell proliferation and induction of cell apoptosis. These results can provide more in-depth understanding about cytotoxic effects of graphene nanostructures which can be functionalized by the proteins of media.

1. Introduction

Graphene, as a single-layer of graphitized carbon atoms, is known as a rising star among the most famous nanostructures, because its unique and fascinating properties have been highly excited fundamental researches [1–3] as well as promising nanotechnology-based applications [4–9]. Recently, graphene-based nanomaterials have been highly induced promising advances in, e.g., biology and medicine including cancer cell targeting, imaging, and therapy [9–14], drug delivery [15–17], antiviral [18], bactericidal [19–23] as well as nematocidal [24] nanomaterials, tissue engineering [25–28], and neural cell and network regeneration [29–33].

In parallel to the bio-applications of graphene-based nanomaterials, their probable toxic effects (such as cytotoxic and even genotoxic effects) on environmental and human health (as almost entirely unfamiliar effects) should be simultaneously investigated for each special case. For instance, Zhang et al. [34] reported concentration- and time-dependent cytotoxicity of graphene in neural phaeochromocytoma-derived PC12 cells, based on reactive oxygen species (ROS) generated by graphene. Chang et al. [35] found although graphene oxide sheets could not enter A549 cells (caused no significant cytotoxicity), it was able to induce a concentration-dependent oxidative stress in the cells resulting in a slight loss of the cell viability at high concentration of ~100 μg/mL. In addition to the ROS generation mechanism, direct contact interaction of extremely sharp edges of graphene with cell wall membrane is known as one of the main mechanisms describing cytotoxicity and even genotoxicity of graphene [19,36]. Wrapping cells within aggregating graphene sheets was also found as another possible mechanism describing cytotoxic effects of graphene sheets in a suspension [37].

In many bio-applications, to obtain biocompatible graphene sheets with lower cytotoxic effects and high stability in biological media, graphene and/or graphene oxide are functionalized with various biocompatible and biostable molecules, such as polyethylene glycol (See, for example, [11]). Moreover, recent investigations demonstrated that upon entrance of nanomaterials (including graphene sheets) into a biological medium, their surfaces are covered by various kinds of biomolecules including proteins. This phenomenon is so-called as "protein corona" [38]. Hence, the type and amount of the associated proteins in the protein corona-graphene composites can significantly affect the potential cytotoxicity of graphene [6]. For example, Hu et al. [39]

* Corresponding author. Tel.: +98 21 66164566; fax: +98 21 66022711.
E-mail address: oakhavan@sharif.edu (O. Akhavan).

http://dx.doi.org/10.1016/j.apsusc.2014.09.155
0169-4332/

found although cytotoxicity of graphene oxide sheets against A549 cells mainly originated from damaging the cell wall membrane (through direct contact interaction with the sheets), fetal bovine serum (FBS) in culture media could soften such destructive interactions.

Recently, cyto- and geno-toxicity of graphene nanoribbons (as elongated strips of single-layer graphene having straight edges and high length-to-width ratio) were studied by our group [40]. But, so far, no investigation has been reported on potential cytotoxicity of protein corona-graphene nanoribbons. Since the toxic effects of graphene-based nanomaterials strongly depends on their size (i.e., lateral dimensions of the sheets or nanoribbons) [36], the cytotoxic effects of protein corona-graphene nanoribbons can be different from the cytotoxic effects of bare graphene sheets [35,36] and also protein corona-graphene sheets [39].

In this work, graphene oxide nanoribbons (GONRs) were synthesized using oxidative unzipping of multi-walled carbon nanotubes (MWCNTs). Concentration-dependent cytotoxicity of protein corona-GONRs (the GONRs functionalized substantially by albumin originated from two different protein sources) on human epithelial cells (A549 cell line) was studied. Although cytotoxicity of bare nanoribbons [40] on stem cells and functionalized (e.g. PEGylated) reduced GONRs on glioblastoma cells [11] were previously studied by our group, this investigation can help to better understanding the cytotoxicity of graphene nanoribbons self-functionalized in culture media (i.e., protein corona-graphene nanoribbons).

2. Experimental

2.1. Synthesis of GONRs

The starting material was MWCNT powder (95% purity, outer diameter of 10–30 nm and length of <5–15 μm [41], provided from io.li.tec). 75 mg of the MWCNTs and 50 mg $NaNO_3$ were added into 75 mL conc. H_2SO_4. After 12 h, 380 mg $KMnO_4$ was added to the mixture. $H_2SO_4$was used to further exfoliate the MWCNTs and also the subsequent ribbons. The suspension was stirred for 1 h at room temperature and then heated in an oil bath at 55 °C for 30 min, at 65 °C for 60 min and finally at 70 °C for 20 min. Then the suspension was removed from the oil bath and allowed to be cooled and stabilized at room temperature. The progress of reactions was determined through color of the solution, so that after completion of the reactions, the color of the solution altered from black to brown, while the green color of permanganate in acid disappeared. The obtained suspension diluted by a deionized (DI) cooled water containing 1 vol% H_2O_2. Then, the suspension was filtered by a polytetrafluoroethylene (PTFE) membrane (5.0 μm pore size) and washed by diluted H_2SO_4, ethanol and finally DI water.

2.2. Material characterization

Surface topography and height profile of the GONRs were examined by atomic force microscopy (AFM; Digital Instruments NanoScope V) in tapping mode. The sample for the AFM imaging was prepared by drop-casting a diluted suspension (10 μg/mL) of the GONR onto a cleaned Si_3N_4/Si(1 0 0) substrate. To deposit the GONRs on the substrate with similar alignments, the droplet was spread over the substrate by repeating unidirectional strokes of a soft paintbrush. After drying the deposited substrate at 100 °C for 1 h, it was washed by DI water in a direction the same as the direction of the brushing. X-ray photoelectron spectroscopy (XPS) was used to study the chemical states of the GONRs. The data were acquired by using a hemispherical analyzer equipped by an Al Kα X-ray source ($h\nu$ = 1486.6 eV) operating at a vacuum better than 10^{-7} Pa. The XPS peaks were deconvolution by using Gaussian components after a Shirley background subtraction. The O/C atomic ratios of the samples were determined using peak area ratio of the XPS core levels and the sensitivity factor (SF) of each element in XPS. Raman spectroscopy was performed at room temperature using a HR-800 Jobin-Yvon with 532 nm Nd-YAG excitation source to study the carbon structure of the GONRs. Samples for XPS and Raman spectroscopy were prepared by casting concentrated suspensions of GONRs onto the substrates and removing the solvents by drying at 100 °C for 1 h. Fourier transform infrared (FTIR) spectroscopy was carried out to study the chemical structure of the GONRs. A FTS 7000 DIGILAB UMA600 spectrometer was used to record the spectra in the range 700–2500 cm^{-1} with 4 cm^{-1} resolution. 256 scans were co-added to improve S/N. Positive and negative ion spectra obtained by ION-TOF IV time-of-flight-secondary ion mass spectrometry (TOF-SIMS), using a 15 kV Bi^+ primary ion source, were acquired at masses up to 500 D, while maintaining the primary ion dose at less than 10^{12} ions/cm^2 to ensure static conditions. All the positive ion spectra were calibrated to the H^+, C^+, CH^+, CH_2^+, CH_3^+, $C_2H_5^+$ and $C_3H_5^+$ peaks and all the negative ion spectra were calibrated to the C^-, C_2^-, CH^-, C_2H^-, C_3^-, C_3H^- peaks before data analysis. Sample spectra were taken over an area 50 μm × 50 μm, with an emission current of 1.0 μA in bunch mode and presented as 128 by 128 pixels.

2.3. Protein corona evaluation

The interactions of the GONRs with both FBS and human plasma serum (HPS) were probed using sodium dodecyl sulfate polyacrylamide gel electrophoresis (SDS-PAGE) approach. Human plasma was obtained from 15 volunteers following the Human Proteome Organization Plasma Proteome Project (HUPO BBB) guidelines [42]. Typically, 100 μL of GONRs (with a concentration of 500 μg/mL) were mixed with 900 μL of FBS or HPS (with two different concentrations of 10% (*in vitro* simulator) and 100% (*in vivo* simulator)), followed by incubation at 37 °C for 1 h. After the incubation time, hard corona-GONRs were obtained by centrifugation. The standard procedure consists of three washing steps before resuspension of the final pellet to the desired concentration. The washing process is designed to remove the excess (unbound or loosely bound) proteins. The hard corona samples were centrifuged (at 4 °C, 20,000 rpm, 50 min) to pellet the GONRs-protein complexes, and the supernatant was carefully removed. The pellet was resuspended in a small amount of phosphate-buffered saline (PBS, with volume of 500 μL) and centrifuged again (at 4 °C, 20,000 rpm, 50 min) to pellet the GONRs -protein complexes. Before the final washing step, the samples were transferred into a low-protein attachment Eppendorf tube, followed by the final centrifugation, and the obtained hard corona GONRs were collected. In order to define the protein profile of hard coronas, 1D SDS-PAGE was employed. For this process, the hard corona GONRs were resuspended in 40 μL of fresh PBS, followed by the addition of 20 μL loading buffer containing 10% Dithiothreitol.

2.4. Cell culture

A549 cell line is one popular cell line in nanotoxicology studies with a cell cycle time of 22 h [43]. A549 cells were purchased from American type culture collection (ATCC, CCL-185). They were cultured in Dulbecco's modified Eagle medium nutrient mixture F-12 Ham (ATCC) supplemented with 10% (v/v) heat-inactivated FBS (Sigma–Aldrich) and 1% penicillin/streptomycin and maintained at 37 °C in humidified 5% CO_2 and 95% air atmosphere.

2.5. Cell viability

The cell viability in terms of mitochondrial integrity, and overall cellular metabolism was measured by alamar blue assay (Invitrogen, Grand Island, NY). A549 cells were plated at 5×10^3 cells per well in 96 well plates, and incubated for 24 h. Before commencing with the assay, old media was replaced with 100 mL of fresh media containing the GONRs with three concentrations mentioned above. The cells were incubated at 37 °C for 24 h. After the incubation period, 10 μL of alamar Blue reagent was added. The plates were again incubated for 30 min at 37 °C. After that, 100 μL of the solution was transferred to an opaque plate. Fluorescence readings of the wells were recorded by a cytofluor fluorescence multi well plate reader (Series H4000 PerSeptive Biosystems, Framingham, MA) with excitation at 530 nm and emission at 580 nm. The cell viability in terms of percent of control cells is expressed as the percent of $(F_{sample}/F_{control}) \times 100$, where F_{sample} is the fluorescence of the cells exposed to the GONRs and $F_{control}$ is the fluorescence of the unexposed control sample. The fluorescence of the wells without any cells was also measured.

2.6. Cell mortality

The cell mortality was evaluated by blue trypan assay. A549 cells were plated in the 12-well plates (1×10^5 cells per well) and incubated for 24 h. Then, the GONRs were incubated with the cells at three different concentrations (10, 50 and 100 μg/mL) in the culture medium. The cells cultured in the free medium were taken as the control. After 24 h, the supernatant was collected and the cells were detached with 250 μL trypsin-ethylenediaminetetraacetic acid solution. The trypsin effect was inhibited with 250 μL of cell culture medium containing FBS. For the cells counting, 100 μL of supernatant each concentration received 20 μL of blue trypan solution. For the detached cells, the same amount (100 μL) received 20 μL of blue trypan solution. After staining, cells were counted using Hemacytometer. The dead cells were stained with blue color. Cell mortality was expressed as the percentage of the dead cells out of the total number of cells for each concentration.

2.7. Apoptosis assay

Hoechst (Hoe) and propidium iodide (PI) were employed to detect living and dead cells. PI (3,8-diamino-5-(3-(diethylmethylamino)propyl)-6-phenyl phenanthridinium diiodide) is very stable fluorescent dye absorbing blue-green light (493 nm) and emitting red fluorescence (630 nm). As a polar compound, it only enters into dead or dying cells having a damaged or leaky cell membrane. Once inside the cell PI interacts with DNA to yield a brightly red fluorescence. PI has been used as a marker of cell damage [44]. Bisbenzimide (Hoe 33342) produces light blue fluorescence when bound to living cells and illuminated with UV light. We used the same culture conditions and GONR exposure as in the case of the test with trypan blue. After GONR exposure, cells were washed two times with PBS, stained with Hoe (0.9 ng/μL in PBS) and incubated for 10 min. After the incubation, cells were washed once with PBS and stained with PI (5 ng/μL in PBS). The plate was mounted and fluorescence images were acquired with an Olympus (1X2-UCB) inverted fluorescent microscope. All images were interfaced and controlled by a PC equipped with a specifically designed software package, utilizing the IPP (Image Pro Plus) as a system environment.

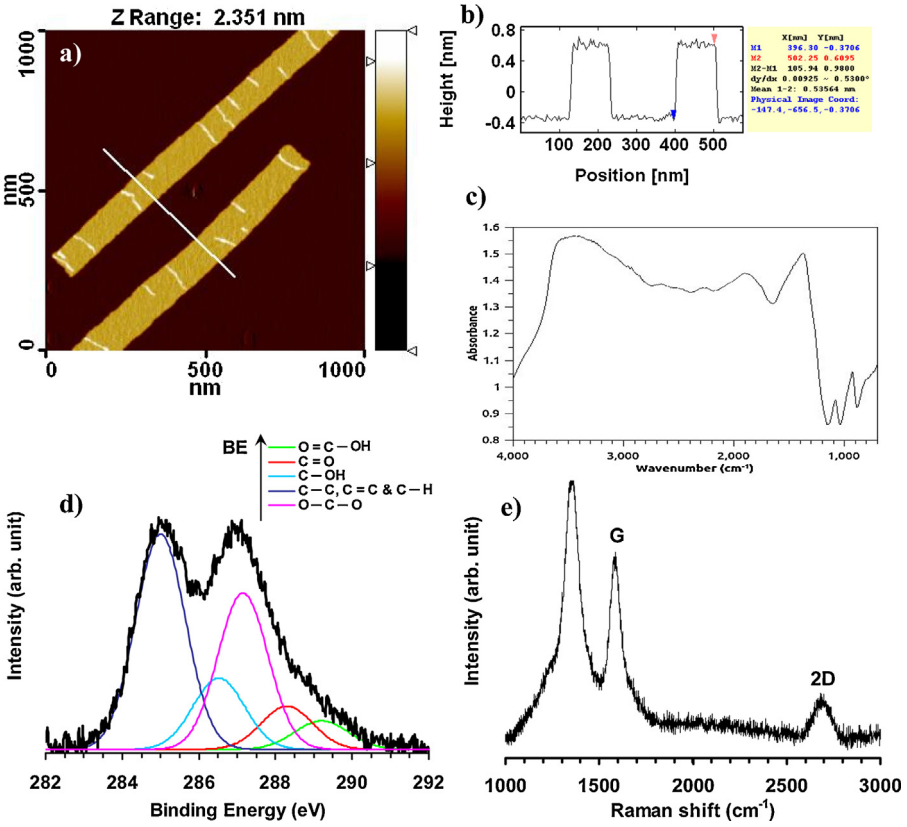

Fig. 1. (a) AFM image of GONRs aligned by a paint-brushing method on Si_3N_4/Si(1 0 0) substrate, (b) height profile of the ribbons marked in the AFM image indicating a thickness equivalent to the thickness of a single-layer GO (~1 nm), and (c) FTIR, (d) C(1s) core level of deconvoluted XP, and (e) Raman spectra of the GONRs.

3. Results and discussion

AFM image of two aligned GONRs with widths of ~100 nm is shown in Fig. 1a. Height profile diagram the GONRs marked in the AFM image (shown in Fig. 1b) indicates that the thickness of the nanoribbons (~1.0 nm) corresponds to the typical thickness of single-layer GO sheets (~0.8 nm) [45]. According to our AFM analysis, abundance of the thicknesses ~1 nm was more than ~75% (among ~50 nanoribbons).

FTIR spectrum of the GONRs is shown in Fig. 1c. The peaks of oxygen functionalities were observed at 3400, 1760, 1300 and 1080 cm^{-1}. According to the paper of Choi et al. [46], these vibrations demonstrate the presence of O—H, C=O, C—OH, and C—O bonds.

The chemical state of the GONRs was studied using XPS. Fig. 1d shows deconvoluted C(1s) peaks of the GONRs. The peak centered at 285.0 eV was assigned to the C—C and C=C bonds. The other peaks centered at the binding energies of 286.5, 287.1, 288.3 and 289.2 eV were assigned to the C—OH, C—O—C, C=O, and O=C—OH oxygen-containing functional groups, respectively (see, e.g., [47]). Based on the SF-modified peak area ratios of the C(1s) and O(1s) core levels, it was found that the O/C ratio of the GONRs was 0.54, which is substantially higher than the oxygen content of the MWCNTs (with O/C ratio of ~0.05).

Raman spectroscopy was utilized to more investigate the carbon structure of the GONRs, as presented in Fig. 1e. The I_D/I_G intensity ratio, originated from the G (~1580 cm^{-1}) and D (~1350 cm^{-1}) bands was found ~1.38. The high value of the I_D/I_G ratio can be assigned to the nearly overall edge defects of the nanoribbons which can also promote increasing the number of smaller aromatic domains. Raman spectra of carbon materials also exhibit a 2D band (described by the adopted double resonant model [48]) sensitive to stacking of graphene sheets [49]. For single-layer graphene, the 2D band locates at 2679 cm^{-1}, while for multilayer graphene (including 2–4 layers) the 2D band appears as a wider peak with 19 cm^{-1} shift to higher wavenumbers [50]. Fig. 1e indicates that the 2D band of the GONRs is around 2680 cm^{-1} implying formation of single-layer nanoribbons.

The characteristic TOF-SIMS peaks were observed in the mass range of 1–70 amu, for both positive and negative spectra. Fig. 2 shows positive and negative ion mode TOF-SIMS high mass resolution spectra of the GONRs. Characteristic peaks observed in the negative mode spectrum include O^- (m/e 16) and OH^- (m/e 17). Impurities, such as Na^+ (m/e 23), and adventitious hydrocarbon fragments were also observed in the positive mode spectrum.

Before incubation of the GONRs with cells, the interactions of the nanoribbons with proteins (protein corona) were evaluated using SDS-PAGE approach. As previous results confirmed the significant role of protein sources in the composition of protein corona [51], we examined two different protein sources including HPS and FBS. According to the protein corona profiles (see Fig. 3), the majority of associated protein in the corona compositions, for both FBS and HPS with the various concentrations, corresponds to albumin (the bands around 70 kDa), as has been proved previously by liquid chromatography-mass spectrometry [52].

The cell viability is examined to estimate the toxicity of the protein corona-GONR samples quantitatively by alamar blue assay (also called prestoblue assay). In this fluorescence-based assay, the non-fluorescent dye Alamar blue (resazurin) acts as an electron acceptor for enzymes like nicotinamide adenine dinucleotide phosphate (NADP), and is converted to a pink fluorescent dye. The amount of non-fluorescence to fluorescence conversion is dependent on the metabolic state of cells. Increased metabolic activity produces more conversion, and hence more fluorescence. Fig. 4ia shows that the viability loss is dose-dependent. At higher GONR

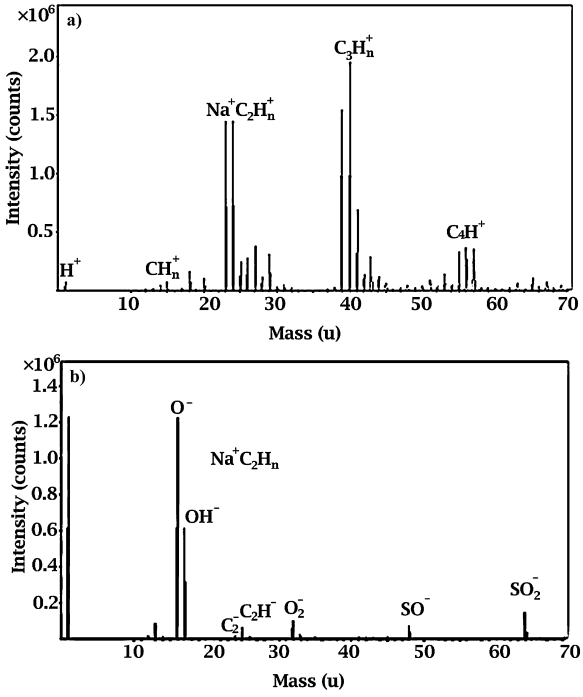

Fig. 2. (a) Positive and (b) negative TOF-SIMS spectra of GONRs.

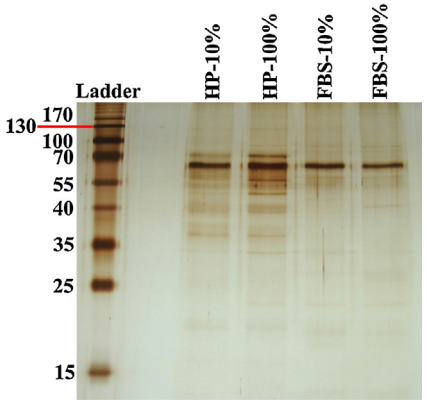

Fig. 3. 15% SDS-PAGE gel of HPS and FBS proteins obtained from GONR-protein complexes free from excess plasma following incubation with human plasma at various concentrations (both 10% and 100%). The molecular weights of the proteins in the standard ladder are reported in terms of kDa on the left for reference.

concentrations (100 μg/mL), a significant viability loss is observed. The viability is only 32% after 24 h post-exposure.

While viability shows the activity of cell mitochondria, the mortality indicates death of the cells. Here, the cell mortality is monitored by trypan blue assay which is based on the principle of dye exclusion to differentiate between living, and dead cells. Living cells with intact cell membranes prevent the trypan blue dye from entering them, whereas dead cells with compromised leaky cell membranes allow the dye to pass through. This allows dead cells stained by the dye to be visualized under a bright field microscope. Fig. 4ib shows the mortality of A549 cells when incubated with the protein corona-GONRs for 24 h. The control (untreated cells) is also included. The average of three independent experiments exhibited a mortality of ~7% for the control and a dose-dependent mortality including ~20 and 58% mortality at 10 and 100 μg/mL concentrations of the GONRs.

Based on nuclear double staining with PI and Hoe (Fig. 4ii), exposure to100 μg/mL of the protein-functionalized GONRs

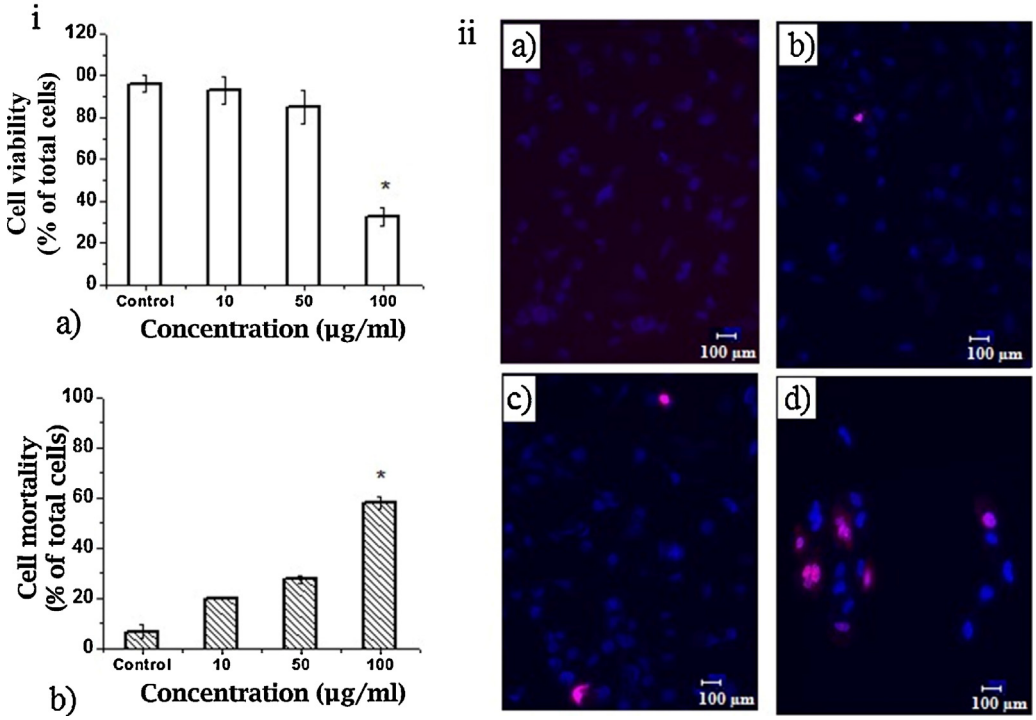

Fig. 4. i Viability (a) and mortality (b) of A549 cells after exposing to the protein corona-GONRs for 24 h. ii Double-staining for Hoe 33342 (blue) and PI (red) in human epithelial cells cultures exposed to the protein corona-GONRs for 24 h at different GONR concentrations: (a) 0 (control), (b) 10, (c) 50, and (d) 100 μg/mL.

significantly decreased the growth and amount of the cells (up to ~60 ± 10% decrease with $p < 0.005$). These images reconfirm the dose-dependent cytotoxicity of the protein corona-GONRs. It is also seen that by increasing the GONR concentration from 10 to 100 μg/mL, not only the cell growth decreased (decreasing the blue color features), but also the interaction of PI with DNA of damaged cells increased (increasing the red color features). The interaction of PI with the damaged cells indicated apoptosis of ~40% of the cells incubated with the GONRs at concentration of 100 μg/mL. The cell apoptosis can be occurred due to the direct contact interaction of the extremely sharp edges of the GONRs with the membrane of cells (as also previously reported for graphene sheets [19,39]). These results also suggest the significant contribution of cell apoptosis (~40%) in decrease of the cell viability (down to ~32%) and increase of the cell mortality (up to ~58%) at the high concentration of GONRs (100 μg/mL). The significant lower toxic property of the GONRs at the lower concentrations (≤50 μg/mL) can be assigned to the lower chance of the GONRs for damaging the cell membrane (lower cell apoptosis and cell mortality) and inhibiting the cell growth (higher cell viability).

4. Conclusions

Concentration-dependent cytotoxicity of GONRs (synthesized through an oxidative unzipping of MWCNTs) was investigated against human epithelial cells in culture media containing FBS or HPS. Incubation of the GONRs in such culture media resulted in formation of protein corona-GONRs (here, GONRs functionalized by albumin, independent from the protein sources used). The protein-functionalized GONRs with concentrations ≤50 μg/mL showed no significant cytotoxicity on the cells. However, the high concentration of 100 μg/mL exhibited significant cytotoxicity resulted in decrease of cell growth and induction of cell apoptosis. These results can provide some more essential and necessary knowledge about interaction of graphene (i.e., protein corona-graphene) with cells in protein-containing culture media and/or body of living organisms. This can also shed light further on upcoming graphene-based nanomedicine.

Acknowledgements

O. Akhavan would like to thank the Research Council of Sharif University of Technology for supporting the work. We also acknowledge GRSTB-FRSQ for supporting T. Javanbakht.

References

[1] Y.B. Zhang, Y. Tan, H.L. Stormer, P. Kim, Experimental observation of quantum Hall effect and Berry's phase in graphene, Nature 438 (2005) 201–204.
[2] K.S. Novoselov, A.K. Geim, S.V. Morozov, D. Jiang, M.I. Katsnelson, I.V. Grigorieva, S.V. Dubonos, A.A. Firsov, Two-dimensional gas of massless Dirac fermions in graphene, Nature 438 (2005) 197–200.
[3] M.I. Katsnelson, K.S. Novoselov, Graphene New bridge between condensed matter physics and quantum electrodynamics, Solid State Commun. 143 (2007) 3–13.
[4] Y.Y. Shao, J. Wang, H. Wu, J. Liu, I.A. Aksay, Y.H. Lin, Graphene based electrochemical sensors and biosensors: a review, Electroanalysis 22 (2010) 1027–1036.
[5] O. Akhavan, E. Ghaderi, R. Rahighi, Toward single-DNA electrochemical biosensing by graphene nanowalls, ACS Nano 6 (2012) 2904–2916.
[6] H.Y. Mao, S. Laurent, W. Chen, O. Akhavan, M. Imani, A.A. Ashkarran, M. Mahmoudi, Graphene: promises, facts, opportunities, and challenges in nanomedicine, Chem. Rev. 113 (2013) 3407–3424.
[7] C. Stampfer, E. Schurtenberger, F. Molitor, J. Güttinger, T. Ihn, K. Ensslin, Tunable graphene single electron transistor, Nano Lett. 8 (2008) 2378–2383.
[8] O. Akhavan, Graphene nanomesh by ZnO nanorod photocatalysts, ACS Nano 4 (2010) 4174–4180.
[9] O. Akhavan, E. Ghaderi, Graphene nanomesh promises extremely efficient in-vivo photothermal therapy, Small 9 (2013) 3593–3601.
[10] J.T. Robinson, S.M. Tabakman, Y. Liang, H. Wang, H. Sanchez Casalongue, D. Vinh, H. Dai, Ultrasmall reduced graphene oxide with high near-infrared absorbance for photothermal therapy, J. Am. Chem. Soc. 133 (2011) 6825–6831.
[11] O. Akhavan, E. Ghaderi, H. Emamy, Nontoxic concentrations of PEGylated graphene nanoribbons for selective cancer cell imaging and photothermal therapy, J. Mater. Chem. 22 (2012) 20626–20633.
[12] K. Yang, J. Wan, S. Zhang, B. Tian, Y. Zhang, Z. Liu, The influence of surface chemistry and size of nanoscale graphene oxide on photothermal therapy of cancer using ultra-low laser power, Biomaterials 33 (2011) 2206–2214.

[13] O. Akhavan, E. Ghaderi, S. Aghayee, Y. Fereydooni, A. Talebi, The use of a glucose-reduced graphene oxide suspension for photothermal cancer therapy, J. Mater. Chem. 22 (2012) 13773–13781.
[14] K. Yang, L. Hu, X. Ma, S. Ye, L. Cheng, X. Shi, C. Li, Y. Li, Z. Liu, Multimodal imaging guided photothermal therapy using functionalized graphene nanosheets anchored with magnetic nanoparticles, Adv. Mater. 24 (2012) 1868–1872.
[15] X. Sun, Z. Liu, K. Welsher, J.T. Robinson, A. Goodwin, S. Zaric, H. Dai, Nano-graphene oxide for cellular imaging and drug delivery, Nano Res. 1 (2008) 203–212.
[16] Z. Liu, J.T. Robinson, X. Sun, H. Dai, PEGylated nanographene oxide for delivery of water-insoluble cancer drugs, J. Am. Chem. Soc. 130 (2008) 10876–10877.
[17] L. Zhang, J. Xia, Q. Zhao, L. Liu, Z. Zhang, Functional graphene oxide as a nanocarrier for controlled loading and targeted delivery of mixed anticancer drugs, Small 6 (2010) 537–544.
[18] O. Akhavan, M. Choobtashani, E. Ghaderi, Protein degradation and RNA efflux of viruses photocatalyzed by graphene-tungsten oxide composite under visible light irradiation, J. Phys. Chem. C 116 (2012) 9653–9659.
[19] O. Akhavan, E. Ghaderi, Toxicity of graphene and graphene oxide nanowalls against bacteria, ACS Nano 4 (2010) 5731–5736.
[20] W. Hu, C. Peng, W. Luo, M. Lv, X. Li, D. Li, Q. Huang, C. Fan, Graphene-based antibacterial paper, ACS Nano 4 (2010) 4317–4323.
[21] O. Akhavan, E. Ghaderi, Escherichia coli bacteria reduce graphene oxide to bactericidal graphene in a self-limiting manner, Carbon 50 (2012) 1853–1860.
[22] J. Ma, J. Zhang, Z. Xiong, Y. Yong, X.S. Zhao, Preparation, characterization and antibacterial properties of silver-modified graphene oxide, J. Mater. Chem. 21 (2011) 3350–3352.
[23] O. Akhavan, E. Ghaderi, Photocatalytic reduction of graphene oxide nanosheets on TiO_2 thin film for photoinactivation of bacteria in solar light irradiation, J. Phys. Chem. C 113 (2009) 20214–20220.
[24] O. Akhavan, E. Ghaderi, K. Rahimi, Adverse effects of graphene incorporated in TiO_2 photocatalyst on minuscule animals under solar light irradiation, J. Mater. Chem. 22 (2012) 23260–23266.
[25] M. Kalbacova, A. Broz, J. Kong, M. Kalbac, Graphene substrates promote adherence of human osteoblasts and mesenchymal stromal cells, Carbon 48 (2010) 4323–4329.
[26] T.R. Nayak, H. Andersen, V.S. Makam, C. Khaw, S. Bae, X. Xu, P.R. Ee, J.H. Ahn, B.H. Hong, G. Pastorin, B. Ozyilmaz, Graphene for controlled and accelerated osteogenic differentiation of human mesenchymal stem cells, ACS Nano 5 (2011) 4670–4678.
[27] W.C. Lee, C.H.Y.X. Lim, H. Shi, L.A.L. Tang, Y. Wang, C.T. Lim, K.P. Loh, Origin of enhanced stem cell growth and differentiation on graphene and graphene oxide, ACS Nano 5 (2011) 7334–7341.
[28] O. Akhavan, E. Ghaderi, M. Shahsavar, Graphene nanogrids for selective and fast osteogenic differentiation of human mesenchymal stem cells, Carbon 59 (2013) 200–211.
[29] S.Y. Park, J. Park, S.H. Sim, M.G. Sung, K.S. Kim, B.H. Hong, S. Hong, Enhanced differentiation of human neural stem cells into neurons on graphene, Adv. Mater. 23 (2011) H263–H267.
[30] N. Li, X. Zhang, Q. Song, R. Su, Q. Zhang, T. Kong, L. Liu, G. Jin, M. Tang, G. Cheng, The promotion of neurite sprouting and outgrowth of mouse hippocampal cells in culture by graphene substrates, Biomaterials 32 (2011) 9374–9382.
[31] C. Heo, J. Yoo, S. Lee, A. Jo, S. Jung, H. Yoo, Y.H. Lee, M. Suh, The control of neural cell-to-cell interactions through non-contact electrical field stimulation using graphene electrodes, Biomaterials 32 (2011) 19–27.
[32] O. Akhavan, E. Ghaderi, Flash photo stimulation of human neural stem cells on graphene/TiO_2 heterojunction for differentiation into neurons, Nanoscale 5 (2013) 10316–10326.
[33] O. Akhavan, E. Ghaderi, E. Abouei, S. Hatamie, E. Ghasemi, Accelerated differentiation of neural stem cells into neurons on ginseng-reduced graphene oxide sheets, Carbon 66 (2014) 395–406.
[34] Y. Zhang, S.F. Ali, E. Dervishi, Y. Xu, Z. Li, D. Casciano, A.S. Biris, Cytotoxicity effects of graphene and single-wall carbon nanotubes in neural phaeochromocytoma-derived PC12 cells, ACS Nano 4 (2010) 3181–3186.
[35] Y. Chang, S.T. Yang, J.H. Liu, E. Dong, Y. Wang, A. Cao, Y. Liu, H. Wang, In vitro toxicity evaluation of graphene oxide on A549 cells, Toxicol. Lett. 200 (2011) 201–210.
[36] O. Akhavan, E. Ghaderi, A. Akhavan, Size-dependent genotoxicity of graphene nanoplatelets in human stem cells, Biomaterials 33 (2012) 8017–8025.
[37] O. Akhavan, E. Ghaderi, A. Esfandiar, Wrapping bacteria by graphene nanosheets for isolation from environment, reactivation by sonication and inactivation by near-infrared irradiation, J. Phys. Chem. B 115 (2011) 6279–6288.
[38] M. Mahmoudi, I. Lynch, M.R. Ejtehadi, M.P. Monopoli, F.B. Bombelli, S. Laurent, Protein-nanoparticle interactions: opportunities and challenges, Chem. Rev. 111 (2011) 5610–5637.
[39] W. Hu, C. Peng, M. Lv, X. Li, Y. Zhang, N. Chen, C. Fan, Q. Huang, Protein corona-mediated mitigation of cytotoxicity of graphene oxide, ACS Nano 5 (2011) 3693–3700.
[40] O. Akhavan, E. Ghaderi, H. Emamy, F. Akhavan, Genotoxicity of graphene nanoribbons in human mesenchymal stem cells, Carbon 54 (2013) 419–431.
[41] O. Akhavan, R. Azimirad, S. Safa, M.M. Larijani, Visible light photo-induced antibacterial activity of CNT-doped TiO_2 thin films with various CNT contents, J. Mater. Chem. 20 (2010) 7386–7392.
[42] A.J. Rai, C.A. Gelfand, B.C. Haywood, D.J. Warunek, J. Yi, M.D. Schuchard, R.J. Mehigh, S.L. Cockrill, G.B. Scott, H. Tammen, P. Schulz-Knappe, D.W. Speicher, F. Vitzthum, B.B. Haab, G. Siest, D.W. Chan, HUPO plasma proteome project specimen collection and handling: towards the standardization of parameters for plasma proteome samples, Proteomics 5 (2005) 3262–3277.
[43] M. Mahmoudi, K. Azadmanesh, M.A. Shokrgozar, W.S. Journeay, S. Laurent, Effect of nanoparticles on the cell life cycle, Chem. Rev. 111 (2011) 3407–3432.
[44] B.W. Kristensen, J. Noraberg, J. Zimmer, Comparison of excitotoxic profiles of ATPA, AMPA, KA and NMDA in organotypic hippocampal slice cultures, Brain Res. 917 (2001) 21–44.
[45] H.C. Schniepp, J.L. Li, M.J. McAllister, H. Sai, M. Herrera-Alonso, D.H. Adamson, R.K. Prud'homme, R. Car, D.A. Seville, I.A. Aksay, Functionalized single graphene sheets derived from splitting graphite oxide, J. Phys. Chem. B 110 (2006) 8535–8539.
[46] E.Y. Choi, T.H. Han, J. Hong, J.E. Kim, S.H. Lee, H.W. Kim, S.O. Kim, Noncovalent functionalization of graphene with end-functional polymers, J. Mater. Chem. 20 (2010) 1907–1912.
[47] O. Akhavan, M. Kalaee, Z.S. Alavi, S.M.A. Ghiasi, A. Esfandiar, Increasing the antioxidant activity of green tea polyphenols in the presence of iron for the reduction of graphene oxide, Carbon 50 (2012) 3015–3025.
[48] A. Ferrari, J. Meyer, V. Scardaci, C. Casiraghi, M. Lazzeri, F. Mauri, S. Piscanec, D. Jiang, K.S. Novoselov, S. Roth, A.K. Geim, Raman spectrum of graphene and graphene layers, Phys. Rev. Lett. 97 (2006) 187401.
[49] L. Malard, M. Pimenta, G. Dresselhaus, M. Dresselhaus, Raman spectroscopy in graphene, Phys. Rep. 473 (2009) 51–87.
[50] D. Graf, F. Molitor, K. Ensslin, C. Stampfer, A. Jungen, C. Hierold, L. Wirtz, Spatially resolved Raman spectroscopy of single-and few-layer graphene, Nano Lett. 7 (2007) 238–242.
[51] S. Laurent, C. Burtea, C. Thirifays, F. Rezaee, M. Mahmoudi, Significance of cell observer and protein source in nanobiosciences, J. Colloid Interface Sci. 392 (2013) 431–445.
[52] H. Mao, W. Chen, S. Laurent, C. Thirifays, C. Burtea, F. Rezaee, M. Mahmoudi, Hard corona composition and cellular toxicities of the graphene sheets, Colloid. Surf. B 109 (2013) 212–218.

Applied Surface Science 320 (2014) 596–601

Contents lists available at ScienceDirect

Applied Surface Science

journal homepage: www.elsevier.com/locate/apsusc

Erratum

Cytotoxicity of protein corona-graphene oxide nanoribbons on human epithelial cells

Doris A. Mbeh[a], Omid Akhavan[b,c,*], Taraneh Javanbakht[a], Morteza Mahmoudi[d], L'Hocine Yahia[a]

[a] Laboratory for Innovation and Analysis of Bio-Performance, École Polytechnique, C.P. 6079, Succursale Centre-ville, Montréal, Québec H3C 3A7, Canada
[b] Department of Physics, Sharif University of Technology, P.O. Box 11155-9161, Tehran, Iran
[c] Institute for Nanoscience and Nanotechnology, Sharif University of Technology, P.O. Box 14588-89694, Tehran, Iran
[d] Department of Nanotechnology, Faculty of Pharmacy, Tehran University of Medical Sciences, Iran

ARTICLE INFO

Article history:
Received 30 August 2014
Received in revised form
23 September 2014
Accepted 23 September 2014
Available online 30 September 2014

Keywords:
Graphene oxide
Nanoribbons
Protein corona
Cytotoxicity

ABSTRACT

Graphene oxide nanoribbons (GONRs) were synthesized using an oxidative unzipping of multi-walled carbon nanotubes. The interactions of the GONRs with various concentrations of fetal bovine serum or human plasma serum indicated that the GONRs were functionalized substantially by the albumin originated from the two different protein sources. Then, concentration-dependent cytotoxicity of the protein-functionalized GONRs on human epithelial cells was studied. Although the GONRs with concentrations ≤50 μg/mL did not exhibit significant cytotoxicity on the cells (with the cell viability >85%), the concentration of 100 μg/mL exhibited significant cytotoxicity including prevention of cell proliferation and induction of cell apoptosis. These results can provide more in-depth understanding about cytotoxic effects of graphene nanostructures which can be functionalized by the proteins of media.

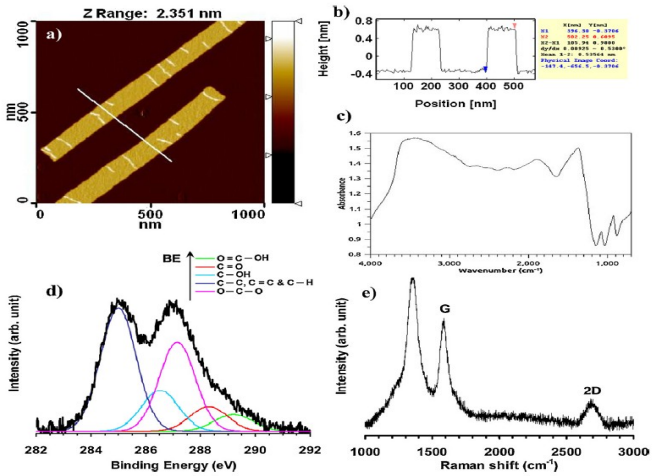

Fig. 1. (a) AFM image of GONRs aligned by a paint-brushing method on Si_3N_4/Si(100) substrate, (b) height profile of the ribbons marked in the AFM image indicating a thickness equivalent to the thickness of a single-layer GO (~1 nm), and (c) FTIR, (d) C(1s) core level of deconvoluted XP, and (e) Raman spectra of the GONRs.

Correct version of Figure 2

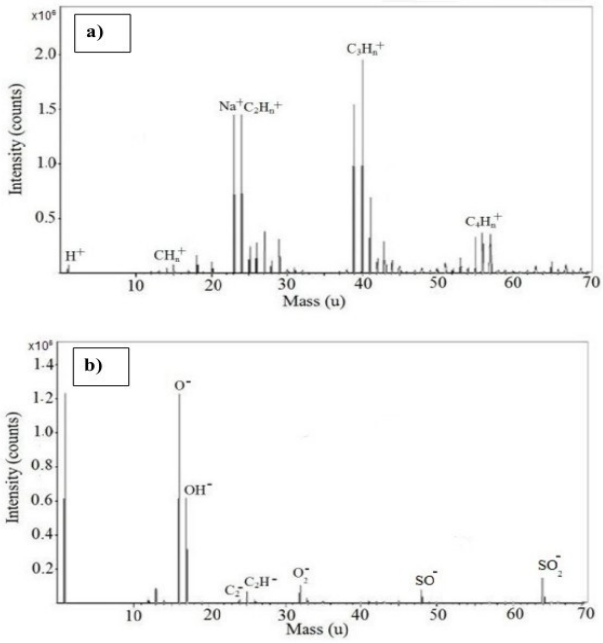

Figure 2. a) Positive and b) negative TOF-SIMS spectra of GONRs.

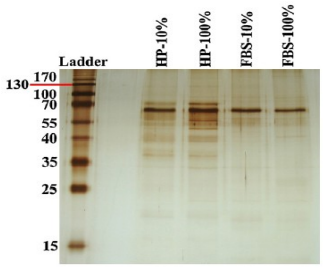

Fig. 3. 15% SDS-PAGE gel of HPS and FBS proteins obtained from GONR–protein complexes free from excess plasma following incubation with human plasma at various concentrations (both 10% and 100%). The molecular weights of the proteins in the standard ladder are reported in terms of kDa on the left for reference.

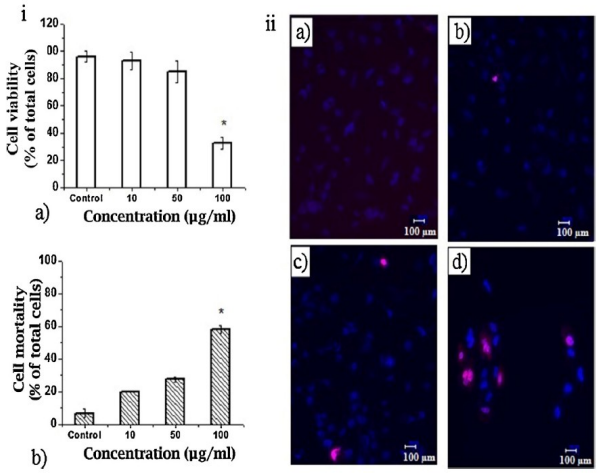

Fig. 4. i Viability (a) and mortality (b) of A549 cells after exposing to the protein corona-GONRs for 24 h. ii Double-staining for Hoe 33342 (blue) and PI (red) in human epithelial cells cultures exposed to the protein corona-GONRs for 24 h at different GONR concentrations: (a) 0 (control), (b) 10, (c) 50, and (d) 100 μg/mL.